Results in Physics 17 (2020) 102996

Contents lists available at ScienceDirect

Results in Physics

journal homepage: www.elsevier.com/locate/rinp

Electrodeposited chromium-doped α-Fe_2O_3 under various applied potential configurations for solar water splitting

Feriel Bouhjar[a,b,d], Lotfi Derbali[c,d,b], Bernabé Marí[a], Brahim Bessaïs[b]

[a] Institut de Disseny i Fabricació, Universitat Politècnica de València, Camí de Vera s/n, 46022 València, Spain
[b] Laboratoire Photovoltaïques, Centre de Recherches et des Technologies de, l'Energie (CRTEn), Technopole, H.lif 2050, Tunisia
[c] Laboratory of Semiconductors, Nanostructures and Advanced Technology, Research and Technology Centre of Energy (CRTEn), Borj-Cedria Science and Technology Park, BP 95, 2050 Hammam-Lif, Tunisia
[d] Department of Physics, College of Sciences and Humanities, Al Quwayiyah, Shaqraa University, Saudi Arabia

ARTICLE INFO

Keywords:
Electrodeposition
α-Fe_2O_3
Cr-doping
XRD analysis
FESEM analysis
Optical properties
Photoelectrochemical properties

ABSTRACT

In this work, high quality hematite (α-Fe_2O_3) Chromium (Cr)-doped thin films have been synthesized via electrodeposition technique, on fluorine-doped tin oxide-coated glass substrates, under various applied potential configurations [cyclic voltammetry (CV), linear sweep voltammetry (LSV) and −0.5 V]. Chromium was added to the electrolyte at such a proportion that the Cr/(Cr + Fe) ratio remained within 8%. The as-deposited films were subsequently annealed in air at 650 °C for 2 h. Our novel study highlights the effect of using variable potential approaches during the film preparation on the properties of Cr-αFe_2O_3 deposited films. The prepared thin films were analyzed by X-ray diffraction, Raman spectroscopy, scanning electron microscopy, UV–Vis absorption and photoelectrochemical (PEC) analysis. XRD revealed that samples are crystallized in Cr-Fe_2O_3 cubic structure with a crystalline orientation in the plane (1 1 1) and a clear improvement of the crystallinity and size crystallite of the Cr-Fe_2O_3 deposited using CV process. SEM micrographs showed that the morphology grains were three-sided pyramid-shaped, expanding with increase of the crystallinity. The calculated band gap values are 2.18, 2.23 and 2.20 eV, respectively for −0.5 V, LSV, CV. The Cr-Fe_2O_3 films synthesized in this study showed high PEC activity with very low carrier density in comparison with the conventionally electrodeposited films. This Cr-doped hematite films 'excellent photoelectrochemical performance was mainly attributed to improved charge carrier properties. Such high photoactivity was attributed to the large active surface area and increased donor density caused by increasing the Cr doping in the α-Fe_2O_3 films.

Introduction

In recent years, semiconductors have attracted the attention of researchers because of their extensive applications in the many fields. Among it, ferrous oxide thin films are widely used due to their excellent n-type semiconducting properties such as a higher absorption coefficient in visible region and a direct energy band gap of 1.9–2.2 eV [1,2]. These characteristics make it a good candidate for solar cell applications [3–5], gas sensing [6], thin-film transistors [7], photocatalysis [8]. α-Fe_2O_3 thin films can be deposited using a variety of techniques such as sol–gel [9], sputtering [10,11], successive ionic layer adsorption and reaction [12], thermal oxidation [13], spray pyrolysis [14] and electrodeposition [15–18]. Among the various deposition techniques, the electrodeposition is one of the simplest techniques due to low-cost and environmentally benign approach, it is having several advantages such as low temperature and ambient pressure processing, it allows to control the crystallization, the morphology and the thickness of the thin films [17]. Several studies reported on the tailoring the morphology, the crystal structure and thickness of the films by adjusting of parameters such as pH and temperature, deposition time and deposition potential [19–21]. Several strategies are being adopted to enhance the performance of hematite photoanodes. Some are nanostructuring of hematite layers [1,21], which use underlayers and overlayers [3], and doping [14]. Doping is considered a powerful route for tuning the charge carrier concentration and to, thereby, modifies the conductivity and catalytic properties of semiconductor metal-oxide photoelectrodes [1,2].

A wide range of elements, which mostly belong to transition metals such as Sn [7], Cu [8], Pt [9], Si [10–13], Ti [14], Al [15], Cd [16], Mo [17], Cr[18] and Ta [19] has been used for doping purposes in hematite films. These dopants influence the conductivity of hematite as well as band gap width, the Fermi level, and charge-transfer processes. However according to the literature, some researchers have reported contradictory effects for doping on photoelectrochemical performance. This apparent discrepancy in the results has been mainly attributed and endorsed to the doping concentration and processing methods. Recently, highly photoactive α-Fe_2O_3 electrodes doped with Pt, Mo, and Cr were prepared by McFarland and Kleiman by the electrodeposition

https://doi.org/10.1016/j.rinp.2020.102996
Received 1 March 2019; Accepted 5 February 2020
Available online 06 February 2020

method [3]. They found that the photoactivity of iron oxide was improved by codeposition with Mo or Cr. The best performing samples were 5% Cr and 15% Mo doped, which had IPCEs at 400 nm of 6% and 12%, respectively, with an applied potential of 0.4 V vs. Ag/AgCl. These IPCE values were 2.2 and 4 times higher than the undoped sample for the 5% Cr and 15% Mo samples, respectively. No evidence was found that improved performance was due to the electrocatalytic effects of the dopant on the surface of the hematite thin film. The main effect of the Mo and Cr dopants is to improve the charge transport properties of hematite so that a bigger fraction of the photon-generated electron/hole pairs is available for surface redox chemistry. In this paper, we have successfully elaborated a high crystalline Cr-doped α-Fe_2O_3 films on FTO substrates using tle electrodeposition technic and discussed the effect of three methods: by a direct linear sweep voltammetry (LSV), cyclic voltammetry (CV) in a range common potential and −0.5 V. The effect of electrochemical approaches on the texture, surface morphology, optical and photoelectrochemical (PEC) property of deposited Fe_2O_3 films was investigated. As far as we are aware, no significant data have been published on the optical, structural and electrical properties of Cr-doped α-Fe_2O_3 films, investigated with different applied electrodeposition potential configurations.

Experimental procedures

Materials and methods

Pure α-Fe_2O_3 films are prepared using a facile and cost-effective electrodeposition process on an FTO (SnO_2/F, 6–8 Ω/sq)-coated glass substrate using a three-electrode cell configuration. The FTO substrates were cleaned ultrasonically in acetone, ethanol and rinsed in distillated water for 15 min and then subsequently dried [1]. The cell contains of a FTO coated glass substrate with (1 × 2) cm^2 of area used as the working electrode, a platinum grid as counter electrode and a saturated calomel electrode (SCE) as the reference electrode.

The three electrodes were in contact with the electrolyte solution that contains $FeCl_3{\cdot}6H_2O$ (5 mM), KF (5 mM), NaCl (0.1 M), and H_2O_2 (1 M). Potassium fluoride was added to the solution to shift the reduction potential from Fe^{3+} to Fe^{2+}, which made it more negative. KCl was used as a supporting electrolyte. The role of H_2O_2 was to produce OH^- during the reduction process by increasing pH in the vicinity of the working electrode surface and to lead to the deposition of iron hydroxides (FeOOH). Furthermore, for doping purposes, different amounts of Cr $(ClO_4)_3$ were used. Cr $(ClO_4)_3$was added to the electrolyte at such a proportion that the Cr/(Cr + Fe) ratio don't exceed the 8%. All the doping percentages reported herein were those of the electrodeposition solution rather than those that exist in electrodeposited and annealed films, unless otherwise indicated. The temperature of bath solution was kept at 60 °C (± 1 °C). Before each electrodeposition step, the precursor solutions were always freshly and cautiously prepared. The Voltalab 40 potentiostat and Volta Master 4 software were used to deposit the thin films. All chemicals were purchased from Sigma-Aldrich and used as received.

Film synthesis process

Cr-Fe_2O_3 thin films were prepared under three electrochemical approaches (configuration): the first approach is to deposit the film by the current method at a definite fixed potential (-0.5). The second is LSV, which consists of varying the potential between two well-defined values in direct direction. The third approach is CV, The process of CV consists of ranging the deposition potential first from an initial value in the positive direction, second reverse to the negative direction and then ended at the starting value.

Film characterization

The crystal structure of the films was investigated through X-ray diffraction using a X'PERT-PRO diffractometer analysis with CuKα radiation (λ = 1.5406 Å) at 40 kV/40 mA at a step rate of 2°/min. The diffraction data was recorded for 2θ values between 20° and 80°. The chemical composition and morphology of the films were examined using an environmental scanning electron microscope (FEIQuanta200) combined with an energy-dispersive X-ray spectrometry detector (EDX). The Raman analyses were performed using a DXR Raman spectrometer with an excitation wavelength of 633 nm. The optical absorbance, the transmittance and gap energy of synthesized films were measured by ultraviolet–visible (UV–Vis) scanning spectrophotometer (JASCO V-730 spectrophotometer). The Mott–Schottky (MS) analysis was performed to determine the conductivity type of Cr-Fe_2O_3 films within the potential range of −200 mV and −600 mV at a frequency of 1000 Hz using autolab PGZ 301 with same cell configuration. The photoconductivity of the prepared Cr-Fe_2O_3 films was studied by PEC analysis. A SCE, a Pt grid and the Cr-Fe_2O_3 films were used as reference, counter and working electrodes, respectively. The geometric surface area of 1 cm^2 was immersed in 0.1 M Na_2SO_4 solution, at room temperature without agitation. A white light source of intensity 150 W was used to illuminate the samples.

Results and discussions

Electrochemical study

To define the deposit potential of the Cr-Fe_2O_3 film, a LSV study was carried out before any deposits of Cr-Fe_2O_3.

Voltammetry experiments were performed on FTO substrates in a solution containing 5 mM $FeCl_3{\cdot}6H_2O$ and KF (5 mM), NaCl (0.1 M), and H_2O_2 (1 M), pH and temperature of the bath were maintained at values 9 and 60 °C, respectively. The scan rate used is 20 mVs^{-1}, and the potential range from −1.2 to +0.2 V vs. SCE. The potential scan was initiated in the negative direction from the open-circuit potential. As shown in Fig. 1, LSV reveals two reduction reactions for Fe^{3+} ions, the voltammogram shows the presence of two cathodic peaks. The first between −0.23 and −0.60 V in which a dimming of the current has been detected. This peak attributed to the reduction of Fe^{2+} ions into Fe^+ as through the reaction (Eq. (1)), the formed Fe^+ ions then react with the OH^- ions in the solution to form the Fe_2O_3 compound (Eq. (2)). The second reduction that start in − 0.83 V is associated with reduction of Fe^+ ions into copper metal (Eq. (3)) [2,3]. Hydrogen

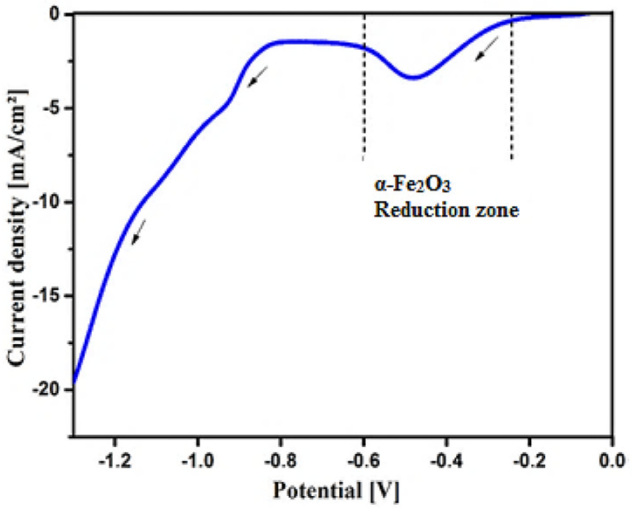

Fig. 1. Linear sweep voltammogram (LSV) for Cr-Fe_2O_3 deposited on FTO substrate, at pH 9 and 60 °C. The scan rate was 20 mVs^{-1}.

evolution was observable when the applied potential was less than −1.2 V (Eq. (4)). These results are in good agreement with previous work that studied the Fe^{2+} ion reductions by the CV method [4,6,22].

$$Fe^{2+} \leftrightarrow Fe^{3+} + e^{-} \quad (1)$$

$$Fe^{3+} + 3OH^{-} \rightarrow Fe_2O_3 + H_2O \quad (2)$$

$$Fe \leftrightarrow Fe^{3+} + 3e^{-} \quad (3)$$

$$2H^{+} + 2\,e^{-} \leftrightarrow H_2 \quad (4)$$

Based on the voltammetry linear studies, different samples of Cr-Fe_2O_3 were electrochemically synthesized using a fixed potential, LSV and CV technique in the potential range of [−0.25 V, −0.5 V]. First sample (Cr-Fe_2O_3-LSV) was prepared by LSV technique starting from −0.5 to −0.25 V with a scan rate Sr = 0.25 mV s^{-1}. The applied potential for sample (Cr-Fe_2O_3–CV) was initialized from −0.5 to −0.25 V and return to the starting potential with a scan rate of 0.5 mV s^{-1}. The third sample was synthesized with fixed potential of −0.5 V with a scan rate of 10 mV s^{-1}. The deposition time was about 15 min for all samples.

Structural analysis

The structure state and the crystalline nature of the Cr-Fe_2O_3 films electrodeposited on the conductive substrate FTO were investigated by XRD analysis. Fig. 2 shows the XRD patterns of Cr-Fe_2O_3 thin films deposited using different approaches by a fixed potential (−0.5 V), LSV and CV. XRD patterns of the deposited Cr-Fe_2O_3 films reveal the presence of polycrystalline Cr-Fe_2O_3 corresponding to cubic structure with the peaks of the FTO substrate and without any secondary phases were observed, neither Fe_2O_3 nor Fe. Apart from the peaks corresponding to the FTO glass, Cr-Fe_2O_3 peaks are at 2θ values of 29.35°, 36.60°, 42.44° and 61.57° corresponding to (1 1 0), (1 1 1), (2 0 0) and (2 2 0) diffraction planes, respectively. This XRD results are in good agreement with the pdf card No.05–0667 of Fe_2O_3 compound. The films deposited using LSV, CV and fixed potential (−0.5 V) methods present the intensity of (1 1 1) peak higher compared to the (1 1 0), (2 0 0) and (2 2 0) planes and it indicates the preferential growth of Cr-Fe_2O_3. Comparing the Fe_2O_3 layers deposited by CV with that at −0.5 V et direct LSV, it was found that film elaborated with the best crystallinity is by CV approach. The crystallite size of the samples deposited was estimated by applying Scherrer formula (Eq. (5)) [7].

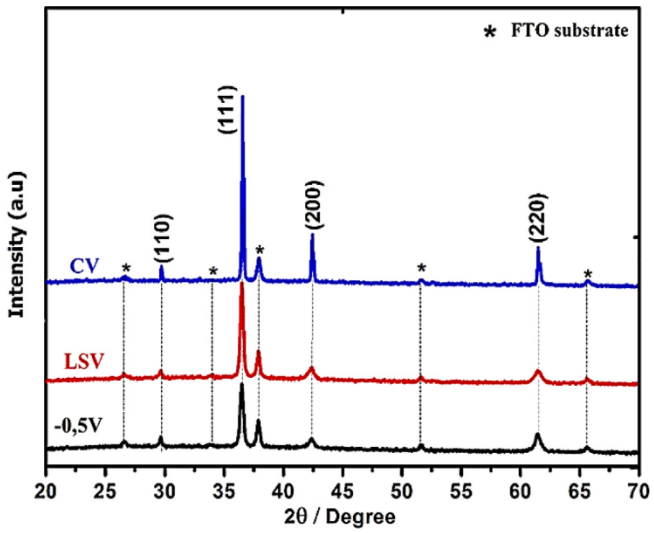

Fig. 2. X-ray diffraction patterns of Cr-Fe_2O_3 thin films deposited using different deposition approaches.

$$D = \frac{0.9\lambda}{\beta cos\theta} \quad (5)$$

where D, λ (0.154060 nm), β and θ were the crystallite size, the wavelength of the X-ray, the full width at half maximum (FWHM) of the peak and the diffraction Bragg's angle, respectively.

From crystallite size values, the dislocation density (δ), and strain (ε) in the films were calculated using Eqs. (6) and (7) and the results are summarized in Table 1.

$$\delta = \frac{1}{D^2} \quad (6)$$

$$\varepsilon = \frac{\beta cos\theta}{4} \quad (7)$$

Table 1 shows that, when the deposition approach changes from −0.5 V to LSV and then to CV, the average crystallite size of the Cr-Fe_2O_3 films has increased from 47 to 69 nm, which confirms the increase in the intensity of the plane (1 1 1) and the decrease of the FWHM. The two values of δ and ε decrease as the size of the crystallites increases, which can be assigned to the decrease of the grain boundaries and defect levels [23].

Raman spectrum analysis

To confirm the high purity of the prepared thin films, Raman response was recorded in the wavelength range from 100 to 800 cm^{-1} as shown in Fig. 3. From the Raman spectra, five peaks appeared at 109, 148, 218, 416 and 636 cm^{-1}, they confirm the formation of Cr-Fe_2O_3 phase in all samples, which are in good agreement with those of XRD. The intense peak at 218 cm^{-1} attributed to second-order Raman allowed mode of the cuprous oxide [9]. The peak located at 109 cm^{-1} is ascribed to the inactive Raman mode [21]. The peak at 148 cm^{-1} may be assigned to Raman scattering from phonons of symmetry Γ_{15}^{-} [21]. In addition to that, the less peak at 416 cm^{-1} is attributed to four-phonon mode $3\Gamma_{12}^{-} + \Gamma_{25}^{-}$ [10]. The peak appearing at 636 cm^{-1} is assigned to the infrared-allowed mode [11]. The Raman spectrums confirm that the film deposited using cyclic voltammetry shows a good crystalline phase in comparison with samples synthetized using LSV and fixed potential (−0.5 V).

Morphological analysis

A SEM micrographs with two magnifications of Cr-Fe_2O_3 thin films deposited using different deposition process of −0.5 V, LSV and CV are shown in Fig. 4a–c, respectively. From the MEB images, it is clear that the shape and size of nanostructures of the obtained films can be related to the deposition process. The all micrographs show clearly that samples present grains with three-face pyramid cover uniformly the surfaces. It is worth noting that when deposition process changes from −0.5 V to LSV and to CV, a noticeable increase in grain size is observed. In fact, the average grain size for the samples of −0.5 V, LSV and CV are 0.5, 0.7 and 0.9 µm, respectively.

It is well known that a Cr-Fe_2O_3 film with larger grains and less grain boundaries are suitable for photovoltaic applications because of the possible reduction of recombination probability at the grain boundaries [12]. Consequently, to obtain a suitable Cr-Fe_2O_3 thin film, the voltammetry approach deposition is a key for controlling the morphologies of the electrodeposited Cr-Fe_2O_3 films. Fig. 5 exhibits the EDAX spectra and cross-section image of Cr-Fe_2O_3 film deposited by CV. From Fig. 5a. it is confirmed the existence of chromium of Cr and O in the layer was 85.74 and 14.26, respectively. The average thickness of this film is about 1.8 µm as shown in Fig. 5b.

Optical properties

The absorption characteristics of the Cr-Fe_2O_3 thin films deposited

Table 1
Nanostructural parameters of the Cr-Fe_2O_3 Thin films deposited using different approaches.

Sample	Lattice parameter a(Å)	FWHM (β) [($\times 10^{-3}$ (rad))]	Crystallite size D (nm)	Dislocation density δ ($\times 10^{-14}$) (lines/m^2)	Strain ε ($\times 10^{-4}$) (lines^{-2}/m^4)
−0.5 V	4.252	3.1	47.1	4.5	7.35
LSV	4.250	3.0	48.2	4.3	7.12
CV	4.249	2.1	69.5	2	4.98

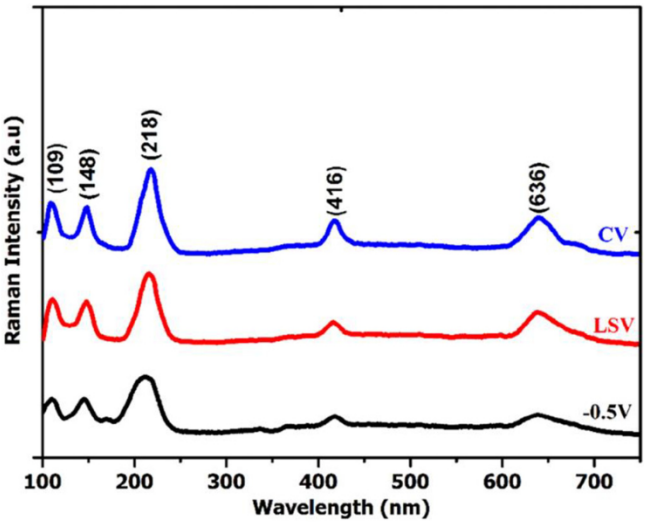

Fig. 3. Raman spectra of Cr-Fe_2O_3 films elaborated by different deposition process (configurations): −0.5 V, LSV and CV.

using different deposition approaches were recorded by UV–Vis spectroscopy to determine the absorption coefficient and the band gap energy in semiconducting thin films [13]. The measurements were taken in the wavelength range of 400–1100 nm. Fig. 6 shows the optical transmittance and absorbance spectra recorded on samples −0.5 V, LSV and CV. It is illustrated that Cr-Fe_2O_3 thin films onto FTO substrates show better absorbance in the range of 400–500 nm.

The thin films absorb highly at wavelengths below 500 nm. It can be observed also that Cr-Fe_2O_3 films have an absorption edge in visible region due to electron transition from valence band to conduction band [19]. No weak transition of Fe_2O_3 materials appear in the transmittance spectra, which implies that the prepared thin films are pure Cr-Fe_2O_3 [14]. The optical measurements such as absorption and transmittance are used to analyze the optical parameters such as optical band gap, absorbance coefficient and nature electron transition of Cr-Fe_2O_3 thin films. The band gap (Eg) of deposited samples can be estimated using the Tauc's formula [14]:

$$(\alpha h\nu)^2 = A\,(h\nu - Eg)$$

where A is a constant, α is the absorption coefficient, h is the Planck's constant, hυ is the photon energy and Eg is the direct band gap energy. The direct band gap energy was obtained by extrapolation of linear line intercepting on x-axis of the plot $(\alpha h\upsilon)^2$ vs. photon energy ($h\upsilon$) as shown in Fig. 7. Linearity in the Tauc plot shows that the optical transition is direct, and the estimated band gap of the Cr-Fe_2O_3 films is 2.18, 2.23 and 2.20 eV for films deposited at −0.5 V, LSV and CV, respectively. These values are very close to those reported in the literature for conventional electrodeposition technique [6,7,9–16,19,21,23].

Conductivity type of Cr-Fe_2O_3 films

To understand the electron transfer mechanism of iron oxide at the interface of electrolyte–electrode, MS analysis was performed [24]. MS approach was used to determine the conductivity type and to estimate the carrier density and flat band potential. The type of the conductivity of the deposited films has been determined from the sign of the MS curves. In fact, the n-type and p-type semiconductor characteristic can be demonstrated using the positive and negative of MS slopes, respectively [24]. The change in space charge capacitance ($1/C_{sc}^2$) with applied potential (E) for the different Cr-Fe_2O_3 samples are shown in Fig. 8. All samples exhibit negative slope of the lines indicates the p-type semiconductivity. The M-S plot used also to estimate the flat band potential (V_{fb}) and the carrier concentration (N_D) of Cr-Fe_2O_3 films according to the MS equation [24]:

$$\frac{1}{C_{sc}^2} = \frac{2}{e\varepsilon\varepsilon_0 N_D A_s^2}\left(E - E_{fb} - \frac{KT}{e}\right)$$

for n-type semiconductor with N_D, A_s^2, C_{sc}, e, ε, ε_0, E, E_{fb}, T and K are carrier density, the capacitance, charge of electron, the relative permittivity, the vacuum permittivity, the applied potential, the flat band potential, the absolute temperature and Boltzmann constant, respectively. The obtained results of carrier densities and the flat band potential values of the Cr-Fe_2O_3 films from the MS measurements are presented in Table 2. The flat band potential is found to be about 0.045, 0.055 and 0.070 V for films deposited at −0.5 V, LSV and CV, respectively. In addition, the acceptor densities in the film were 2.90×10^{17}, 2.85×10^{17} and 2.68×10^{17} cm^{-3}, respectively under the different electrodeposition configurations used in our study.

These values are in line with the previously reported values for Cr-Fe_2O_3 films synthesized through different methods [25,26]. The Cr-Fe_2O_3 film deposited using CV approach has the lowest carrier density, indicating the presence of a minimal number of defect sites. The photoconductivity of films prepared was studied by PEC analysis. A SCE, a Pt grid and the Cr-Fe_2O_3 films were used as the reference counter and

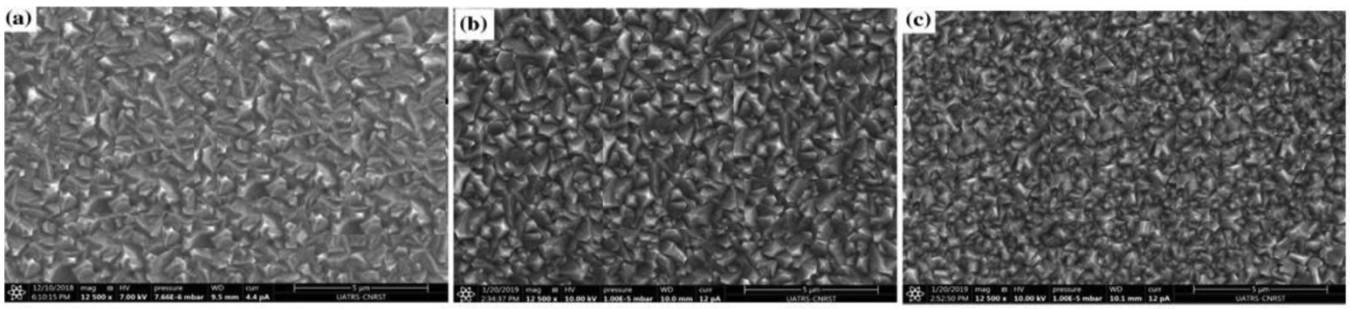

Fig. 4. SEM morphology of Cr-Fe_2O_3 samples deposited using different approaches (a) −0.5 V, (b) LSV and (c) CV.

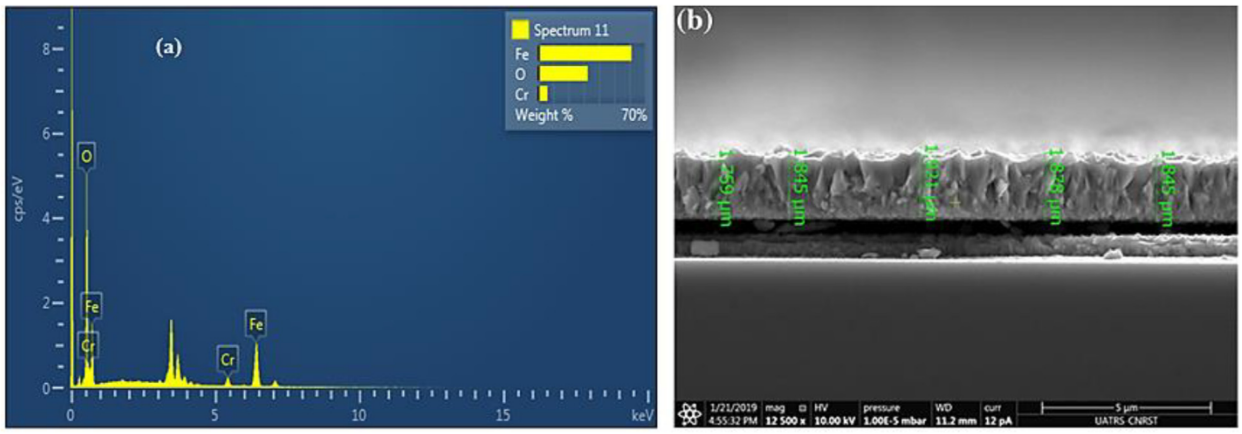

Fig. 5. (a) EDAX spectrum and (b) cross-section image of Cr-Fe_2O_3 film synthesized using the CV process.

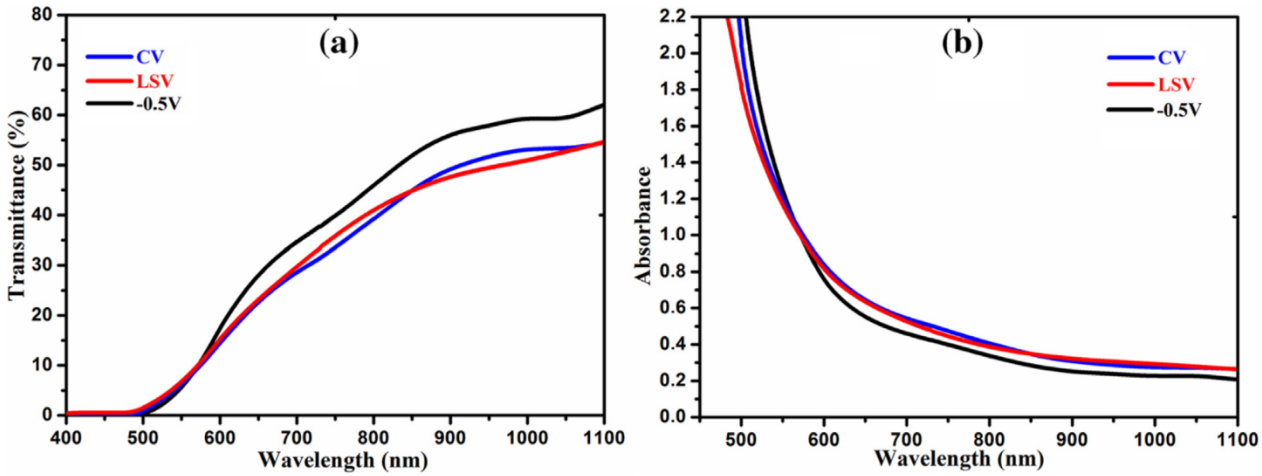

Fig. 6. Transmittance (a) and absorbance (b) spectra of Cr-Fe_2O_3 thin films deposited using different deposition approaches: −0.5 V, LSV and CV.

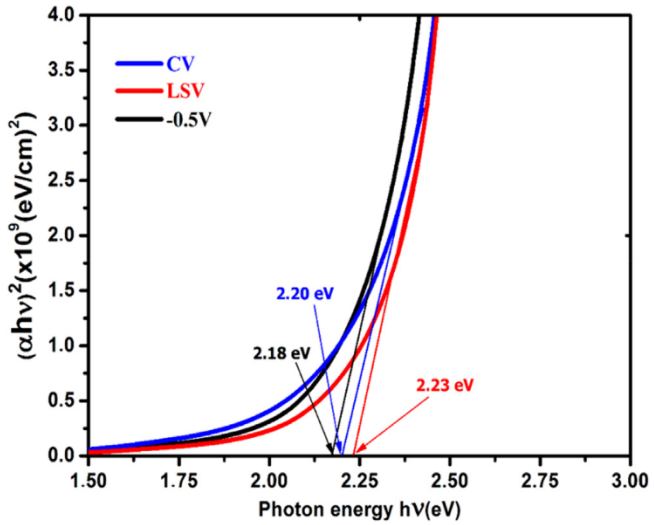

Fig. 7. Plots of $(\alpha h\upsilon)^2$ vs. $(h\upsilon)$ for the electrodeposited Cr-Fe_2O_3 thin films onto FTO glass substrates using different voltammetry techniques.

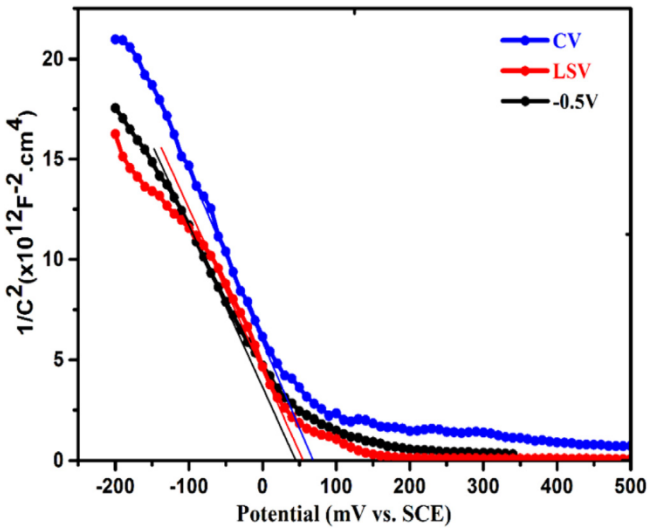

Fig. 8. MS plots of Cr-Fe_2O_3 on FTO substrates deposited using different processes of −0.5 V, LSV and CV in presence of 0.1 M Na_2SO_4 electrolytes (pH 4.9).

working electrodes, respectively. The prepared thin films were immersed in 0.1 M Na_2SO_4 solution, at 25 °C [27–30]. A white light intensity lamp of 150 W was used to illuminate the samples. The photocurrent measurements can give the information about the charge carriers. Fig. 9 exhibits the photocurrent response of the Cr-Fe_2O_3 films deposited by CV, LSV and at −0.5 V. Upon illumination, the photoelectrochemical response shows a moderate anodic photocurrent for all prepared samples indicating that the Cr-Fe_2O_3 films having p-type conductivity, which confirms the results of MS studies. The photocurrent study shows that the Cr-Fe_2O_3 deposited by CV has the best

Table 2
Carrier densities and flat band potentials of Cr-Fe_2O_3 films deposited at different applied potential configurations: −0.5 V, LSV and CV.

Electrodeposition process	Conductivity type	Carrier (density/cm^{-3})	Flat band (potential/V)
−0.5 V	n-type	2.90×10^{17}	−0.045
LSV	n-type	2.85×10^{17}	−0.055
CV	n-type	2.68×10^{17}	−0.070

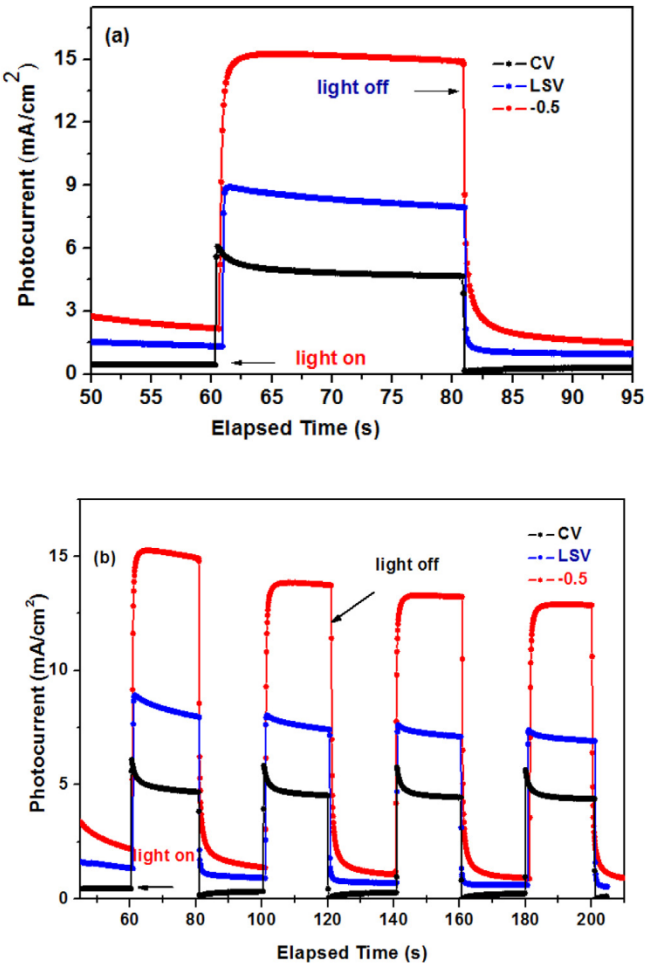

Fig. 9. (a) The photocurrent intensity for the Cr-doped Fe_2O_3 electrodes under on/off illumination conditions, measured in the electrolyte with a bias potential of +0.1 V, (b) The time dependence of the photocurrent intensities for the Cr-doped α-Fe_2O_3 electrodes in successive illumination cycles.

photocatalytic activity.

Conclusion

In summary, high quality Cr-Fe_2O_3 films were deposited via electrochemical deposition technique under various configuration including sweep voltammetry technique. The effect of the deposition approach was investigated in details. The XRD patterns revealed that the films deposited using the cyclic and sweep voltammetry process showed good crystalline in nature. SEM images show three-sided pyramid shaped morphology grains, and the grains have become larger with increase of crystallinity, this result is consistent with XRD. The optical properties revealed that all films have a direct band gap value was estimated to be between 2.1 and 2.3 eV. MS measurements display that the films deposited are n-type semiconductors, the carrier density values at around 10^{17} cm^{-3} are in good agreement with those reported in the literature. The Cr-Fe_2O_3 films deposited using CV and LSV exhibit superior photocurrent. These facile electrochemical approaches were expected to extend the preparation of pure cuprous oxide phase that can be used to develop high quality optoelectronic devices.

Acknowledgements

This work was supported by the Ministry of High Education and Scientific Research (Tunisia), the Ministry of Economy and Competitiveness (Spain) (ENE2016-77798-C4-2-R) and the Generalitat Valenciana (Prometeus 2014/044).

References

[1] Warren SC, Voïtchovsky K, et al. Identifying champion nanostructures for solar water-splitting. Nat Mater 2013;12:842–9. https://doi.org/10.1038/NMAT3684.
[2] Beermann N, Vayssieres L, Lindquist SE, Hagfeld A. Photoelectrochemical studies of oriented nanorod thin films of hematite. J Electrochem Soc 2000;147:2456–61. https://doi.org/10.1149/1.1393553.
[3] Steier L, Herraiz-Cardona I, et al. Understanding the role of underlayers and overlayers in thin film hematite photoanodes. Adv Funct Mater 2014;24:7681–8. https://doi.org/10.1002/adfm.201402742.
[4] Bak A, Choi SK, Park H. Photoelectrochemical performances of hematite (α-Fe2O3) films doped with various Metals. Photoelectrochemical Bull Korean Chem Soc 2015;36:1487–94. https://doi.org/10.1002/bkcs.10290.
[5] Zandi O, Hamann TW. The potential versus current state of water splitting with hematite. Phys Chem Chem Phys 2015;17(35):22485–503. https://doi.org/10.1039/C5CP04267D.
[6] Morin FJ. Electrical properties of α-Fe2O3 and α-Fe2O3 containing titanium. Phys Rev 1951;83:1005. https://doi.org/10.1103/PhysRev.83.1005.
[7] Arakelyan VM, Aroutiounian VM, et al. Photoelectrochemistry of tin-doped iron oxide electrodes. Sol Energy 2007;81:1369–76. https://doi.org/10.1016/j.solener.2007.01.006.
[8] Jang JS, Lee J, Ye H, Fan FRF, Bard AJ. Rapid screening of effective dopants for Fe2O3 photocatalysts with scanning electrochemical microscopy and investigation of their photoelectrochemical properties. J Phys Chem C 2009;113:6719–24. https://doi.org/10.1021/jp8109429.
[9] Kleiman-Shwarsctein A, Hu YS, et al. Pt-doped r-Fe2O3 thin films active for photoelectrochemical water splitting. Chem Mater 2008;20:3803–5. https://doi.org/10.1021/cm800144q.
[10] Cesar I, Kay A, Gratzel M, Martinez JAG. New benchmark for water photooxidation by nanostructured α-Fe2O3 films. J Am Chem Soc 2006;128:15714–21. https://doi.org/10.1021/ja064380l.
[11] Saremi-Yarahmadi S, Wijayantha KGU, Tahir AA, Vaidhyanathan B. Nanostructured α-Fe2O3 electrodes for solar driven water splitting: effect of doping agents on preparation and performance. J Phys Chem C 2009;113:4768. https://doi.org/10.1021/jp808453z.
[12] Liang YQ, Enache CS, Krol R. Photoelectrochemical characterization of sprayed α-Fe2O3 thin films: influence of Si doping and SnO2 interfacial layer. Int J Photoenergy 2008. https://doi.org/10.1155/2008/739864. Article ID 739864.
[13] Cesar I, Sivula K, Kay A, Zboril R, Gratzel M. Influence of feature size, film thickness, and silicon doping on the performance of nanostructured hematite photoanodes for solar water splitting. J Phys Chem C 2009;113:772–82. https://doi.org/10.1021/jp809060p.
[14] Kleiman-Shwarsctein A, Hu YS, Stucky GD, McFarland EW. Improved photoelectrochemical performance of Ti-doped α-Fe2O3 thin films by surface modification with fluoride. Chem Commun 2009:2652–4. https://doi.org/10.1039/b901135h.
[15] Sivula K, Le Formal F, Grätzel M. Solar water splitting: progress using hematite (α-Fe2O3) photoelectrodes. ChemSusChem 2011;4(4):432–49. https://doi.org/10.1002/cssc.201000416.
[16] Bak A, Choi W, Park H. Enhancing the photoelectrochemical performance of hematite (α-Fe2O3) electrodes by cadmium incorporation. Appl Catal 2011;B110:207–15. https://doi.org/10.1016/j.apcatb.2011.09.002.
[17] Kleiman-Shwarsctein A, Forman AJ, Hu YS, McFarland EW, Stucky GD. Electrodeposition of α-Fe2O3 doped with Mo or Cr as photoanodes for photocatalytic water splitting. J PhysChem C 2008;112:15900–7. https://doi.org/10.1021/jp803775j.
[18] Bouhjar F, Mollar M, Chourou ML, Marí B, Bessaïs B. Hydrothermal synthesis of nanostructured Cr-doped hematite with enhanced photoelectrochemical activity. Electrochim Acta 2018;260:838–46. https://doi.org/10.1016/j.electacta.2017.12.049.
[19] Akl AA. Optical properties of crystalline and non-crystalline iron oxide thin films deposited by spray pyrolysis. Appl Surf Sci 2004;233:307–19. https://doi.org/10.1016/j.apsusc.2004.03.263.
[20] Tilley SD, Cornuz M, Sivula K, Grätzel M. Light-induced water splitting with ematite: improved nanostructure and iridium oxide. Catalysis Angew Chem 2010;122:6549–52. https://doi.org/10.1002/ange.201003110.
[21] Sivula K, Formal FL, Grätzel M. Solar water splitting: progress using hematite (α-Fe_2O_3) photoelectrodes. ChemSusChem 2011;4:432–49. https://doi.org/10.1002/cssc.201000416.
[22] Zandi O, Hamann TW. The potential versus current state of water splitting with

hematite. Phys Chem Chem Phys 2015;17:22485–503. https://doi.org/10.1039/C5CP04267D.
[23] Jang JS, Lee J, Ye H, Fan FRF, Bard AJ. Rapid screening of effective dopants for Fe2O3 photocatalysts with scanning electrochemical microscopy and investigation of their photoelectrochemical properties. J Phys Chem C 2009;113:6719–24. https://doi.org/10.1021/jp8109429.
[24] Jaramillo TF, Baeck SH, et al. Automated electrochemical synthesis and photoelectrochemical characterization of Zn1-xCoxO thin films for solar hydrogen production. J Comb Chem 2005;7:264–71. https://doi.org/10.1021/cc049864x.
[25] Jaramillo TF, Baeck SH, et al. Macromol combinatorial electrochemical synthesis and screening of mesoporous ZnO for photocatalysis. Rapid Commun 2004;25:297–301. https://doi.org/10.1002/marc.200300187.
[26] Miller EL, Paluselli D, Marsen B, Rocheleau RE. Low-temperature reactively sputtered iron oxide for thin film devices. Thin Solid Films 2004;466:307–13. https://doi.org/10.1016/j.tsf.2004.02.093.
[27] Belkhedkar MR, Ubale AU. Preparation and characterization of nanocrystalline α-Fe2O3 thin films grown by successive ionic layer adsorption and reaction method. Int J Mater Chem 2014;4:109–16. https://doi.org/10.5923/j.ijmc.20140405.02.
[28] Shinde SS, Bansode RA, Bhosale CH, Rajpure KY. Physical properties of hematite α-Fe2O3 thin films: application to photoelectrochemical solar cells. J Semicond 2011;32:1–8. https://doi.org/10.1088/1674-4926/32/1/013001.
[29] Souza FL, Lopes KP, Nascente PAP, Leite ER. Nanostructured hematite thin films produced by spin-coating deposition solution: application in water splitting. Sol Energy Mater Sol Cells 2009;93:362–8. https://doi.org/10.1016/j.solmat.2008.11.049.
[30] Amin YM, Sookhakian M, et al. A layer-by-layer assembled graphene/zinc sulfide/polypyrrole thin-film electrode via electrophoretic deposition for solar cells. Thin Solid Films 2014;552:204–11. https://doi.org/10.1016/j.tsf.2013.12.019.